Electronic Supplementary Information

Chiral Superstructure of Aragonite Similar to *Turritella terebra* Shell Induced by CTAB's adsorption chirality

Xin Yang[a], Xun Liu[a,d,*], Fujun Yao[a], Lingyuan Chen[a], Wenyuan Hu[b,d], Jiawen Li[c], Zheng Kang[c], Xiaohui Duan[a], Chonghua Pei[a*]

[a] *State Key Laboratory of Environment-Friendly Energy Materials, Southwest University of Science and Technology, Mianyang 621010, PR China.*

[b] *School of Material and Chemistry, Southwest University of Science and Technology, Mianyang 621010, PR China.*

[c]*Radioactive Waste Technology and Radiochemistry Research Department, China. Nuclear Power Technology Research Institute Co., Ltd, Shenzhen, 518000, PR China.*

[d] *National Health Commission Key Laboratory of Nuclear Technology Medical Transformation, Mianyang Central Hospital, Mianyang 621010, P. R. China*

*Corresponding authors.

Email addresses:

Xun Liu: liuxun@swust.edu.cn

Chonghua Pei : peichonghua@swust.edu.cn

The Electronic Supplementary Information including experiments and characterizations, Figs. S1-S13, relevant explanations of some figures, Tables S1-S6, and References.

Table of Contents
(Arranging according to the sequence of relevant contents in the main text)

Fig. S1 Molecular Structure Formula of CTAB

Text S1: Experiments and characterizations

Fig. S2 Schematic diagram of the experimental setup

Fig. S3 The influence of Mg^{2+} and CTAB concentration on the phase

Fig. S4 Mapping images of A-$CaCO_3$

Text S2: Effects of different Mg^{2+} and CTAB concentrations on crystal form

Fig. S5 Effects of different Mg^{2+} and CTAB concentrations on morphology

Text S3: Effects of different Mg^{2+} and CTAB concentrations on morphology

Fig. S6 SEM images of the two enantiomers of A-$CaCO_3$ (upper), and their horizontal triple magnification (down)

Fig. S7 CD Spectra of organic matter extracted from *Turritella terebra* Shell and *Turritella terebra* Shell without organic matter in it

Fig. S8 An asymmetric spherical crown structure

Fig. S9 HRTEM images of different crystal planes

Fig. S10 Adsorption simulation of CTAB molecules on different aragonite crystal planes (upper) and chiral enantiomers formed by absorption of CTAB molecules on (0 2 2) crystal planes (upward view) (down)

Fig. S11 Adsorption simulation of CTA^+ on different aragonite crystal planes

Fig. S12 Adsorption simulation of OTAB molecules on different aragonite crystal planes

Fig. S13 Schematic diagram of the deviation of "daughter" particles as they adhere to "mother" particles as caused by adsorption chirality

Table S1 Binding energy and deformation energy of CTAB on different aragonite crystal planes

Table S2 Energy of CTAB adsorbed on calcium carbonate (0 2 2) crystal plane

Table S3 Energy of CTAB adsorbed on calcium carbonate (0 2 1) crystal plane

Table S4 Energy of CTAB adsorbed on calcium carbonate (0 1 2) crystal plane

Table S5 Bond length of different N-CH_3 bonds on the head group of CTA^+

Table S6 Bond length of different N-CH_3 bonds on the head group of OTAB molecule

References

Fig. S1

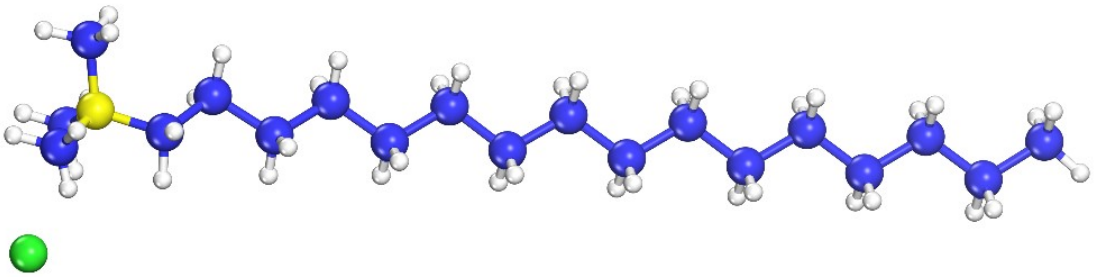

Fig. S1 Molecular Structure Formula of CTAB.

Text S1: Experiments and characterizations

Experiments

Synthesize the twisted dumbbell-like pure aragonite.

All chemicals used in the experiment, including CTAB, anhydrous $CaCl_2$, $MgCl_2 \cdot 6H_2O$, anhydrous ethanol (purchased from Aladdin), and NH_4HCO_3 (purchased from Chengdu Kelong Chemical Co., Ltd.), are analytical grade. Ultrapure water is self-made in the laboratory, with a resistivity of 18.25 MΩ· cm.

Gas diffusion was used to mineralize $CaCO_3$.[1] First, a mixed aqueous solution of $CaCl_2$ and $MgCl_2$ was prepared for standby. The concentration of $CaCl_2$ was fixed at 0.01 mol·L^{-1}, while for comparison that of $MgCl_2$ was varied from 0.01 mol·L^{-1} to 0.04 mol·L^{-1}. An appropriate amount of CTAB was added to 100 mL of the above mixed aqueous solution. The mixture was next transferred into a smaller crystallizing dish (*Φ* 10 cm), which was then put into a larger crystallizing dish that contained 5 g of NH_4HCO_3 (*Φ* 12 cm). The larger dish was sealed with plastic wrap secured by a rubber band. Mineralization was carried out at room temperature (about 20 °C) for a certain time. This improvised experimental device is shown in Fig. S2.

As necessary, liquid nitrogen was used to quickly cool the mixture during the reaction in order to investigate intermediate stages in the process. After the reaction was complete, the white precipitate at the bottom of the small crystallizing dish was filtered using suction, and the filtrate was cleaned 3-5 times using ultrapure water and absolute ethanol, respectively, and then freeze-dried for standby. The concentration of

CTAB varied from 0 $g \cdot L^{-1}$ to 10 $g \cdot L^{-1}$.

Extraction of organic from *Turritella terebra* Shell.

The protein in the shell was extracted by acid dissolution, which was divided into two steps: protein extraction and protein purification.[2, 3]

Prepare 100 ml of 20 % acetic acid solution, and add dithiothreitol (DTT) to the solution to a concentration of 5 mM. Weigh 20 g of shell powder, and slowly add it into the prepared solution to avoid violent dissolution leading to explosive boiling of the solution. To protect the protein, all dissolution was carried out in a constant temperature bath at 4 °C. During dissolution, $[CH_3COO^-]$: $[Ca^{2+}]$ was always larger than 2:1, and the solution was stirred for 72 h to ensure sufficient dissolution. Then, centrifuge the solution at 5000 rpm for 10 min to remove the partially dissolved shell powder and impurities. The supernatant was filtered by suction using an aqueous phase filter membrane of 0.45 μm to remove insoluble organic matter. The filtrate was stored in a refrigerator at 4 °C for subsequent dialysis purification.

A dialysis bag with a length of 200 mm, a width of 77 mm and a retention molecular weight of 1000 D was used for protein purification. Before use, immerse the dialysis bag in 30% ethanol aqueous solution for 20 min, then clean the impurities on both sides of the dialysis bag, and then clean it with ultrapure water for three times, dry it naturally, put it into a self-sealing bag, and store it at room temperature. Before dialysis, soak the cleaned dialysis bag in ultrapure water for 5 minutes.

During dialysis, gloves should be used to avoid contamination. Clamp one end of the dialysis bag and ensure no leakage. Then, move the extracted solution into the dialysis bag, squeeze out the air above, clamp the other end of the dialysis bag, and check the sealing of the dialysis bag by squeezing. Put the dialysis bag into a beaker containing deionized water and perform dialysis at 4 °C. Change deionized water every four hours and repeat dialysis for five times to ensure the dialysis effect. After dialysis, take 10 ml of protein dialysate for qualitative analysis.

Preparation of *Turritella terebra* Shell without organic matter.

In order to remove the organic matter in the *Turritella terebra* Shell, an anionic

surfactant Sodium dodecyl sulfate (SDS) was used.[4, 5] 10 mL SDS aqueous solution with mass fraction of 0~3% was prepared at room temperature, and then 0.2 g of crushed shell powder was added into the solution. Dissolution of organic matter was under stirring condition for 2 hours. After stirring, undissolved solid powder was filtered out by suction, and then cleaned with absolute ethanol for 2-3 times and with ultrapure water for 3-4 times in turn. Finally, freeze dry the sample for later use.

Characterizations

The phase of the sample was analyzed using an X-ray diffractometer (Panaco, from the Netherlands). The working voltage and current were 40 kV and 40 mA respectively. Cu target Kα radiation with a λ of 1.54187 Å was applied. The step interval was 0.03°, the scanning speed was 10° ·min^{-1}, and the scanning range was 3°-80°. The morphology and particle size of the $CaCO_3$ particles were characterized using a TESCAN MIRA3 (LMU) field emission scanning electron microscope (TESCAN Company, from the Czech Republic) under 10 kV accelerating voltage, and the samples were characterized by mapping with a high resolution cold field emission scanning microscope (UItra55). During characterization, Au was plated on all sample surfaces to increase their conductivity. The samples were also tested using a Fourier transform infrared spectrometer FT-IR5700 (Bruker, from Germany). The content of CTAB in the $CaCO_3$ precipitate was determined using a synchronous thermal analyzer STA449FS (NETZSCH, from Germany) at temperatures ranging from ambient to 1000 °C. The microstructure of $CaCO_3$ was inspected using a JEOL JEM-100 CXII transmission electron microscope (TEM, from Japan) at 80 kV and room temperature. At room temperature, the samples were analyzed using a circular dichroism chromatograph J-1500 (JASCO, from Japan) at a working scanning rate of 50 nm·min^{-1} and a data interval of 0.1 nm.

Statistics of twist direction

With the aid of scanning electron microscope (with a magnification of 650), the distortion directions of 100 particles were counted. Among them, 33 particles could not be determined due to the angle of view. Among the 67 particles effectively counted,

there were 32 left-handed particles and 35 right-handed particles, with a ratio of about 1:1.

Theoretical simulation

Establish aragonite cell, cut crystal planes (022), (021) and (012), and then expand them into 6 × 3, 6 × 2 and 6 × 2 super crystal planes respectively. Construct the molecular model of CTAB, CTA^+ and OTAB, then optimize their using molecular mechanics. The Adsorption Location module in the Materials Studio platform,[6, 7] the "Simulated annexing" simulation method, the "fine" precision, and the Compass force field are used for simulation. The calculation methods of static electricity and van der Waals force are respectively "Ewald" and "Atom based".

Fig. S2

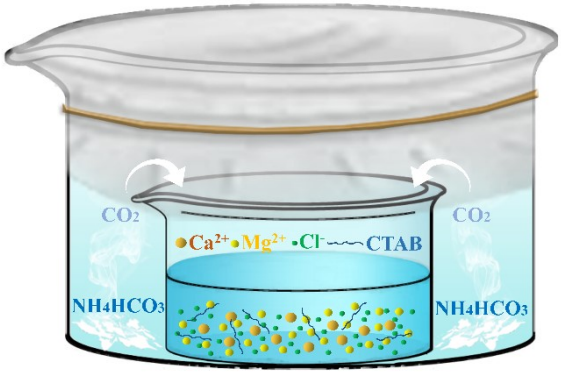

Fig. S2 Schematic diagram of the experimental setup.

Fig. S3

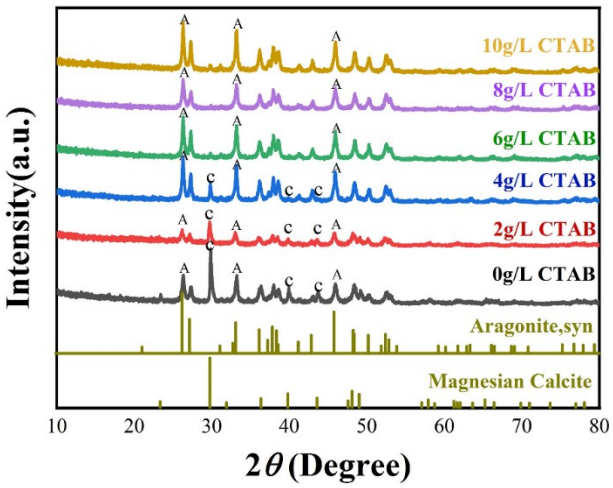

Fig. S3 The influence of Mg^{2+} and CTAB concentration on the phase.

Fig. S4

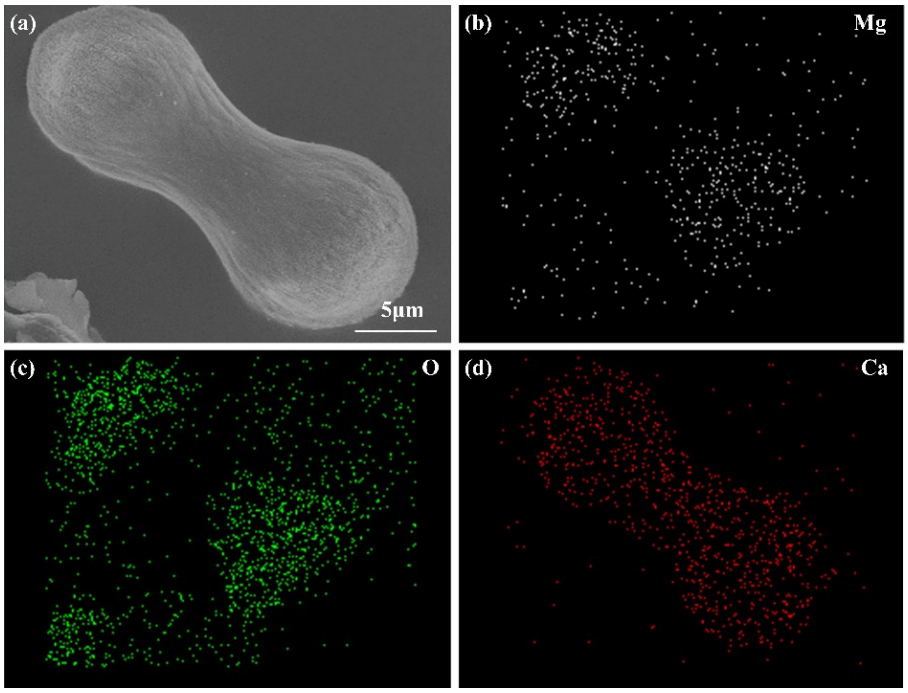

Fig. S4 Mapping images of A-$CaCO_3$.

Text S2: Effects of different Mg^{2+} and CTAB concentrations on crystal form

Coordinated regulation by Mg^{2+} and CTAB, with Mg^{2+} playing a dominant role, controls the formation of the aragonite. During the experiment, we compared the effects of different Mg^{2+} and CTAB concentrations on the forms of the crystals in the mineralized products. If CTAB alone is used, a mixed phase of calcite and vaterite results at low concentrations of CTAB. As the concentration of CTAB increases, there is a gradual shift to pure vaterite (Fig. S3). If Mg^{2+} is used, the aragonite phase forms, but a certain amount of calcite phase is mixed with it. If CTAB is added, calcite formation is inhibited to some extent, and a pure aragonite phase can be obtained in the end (Fig. S3). The mapping image shows that the Mg^{2+} is evenly distributed in A-$CaCO_3$ (Fig. S4).

Fig. S5

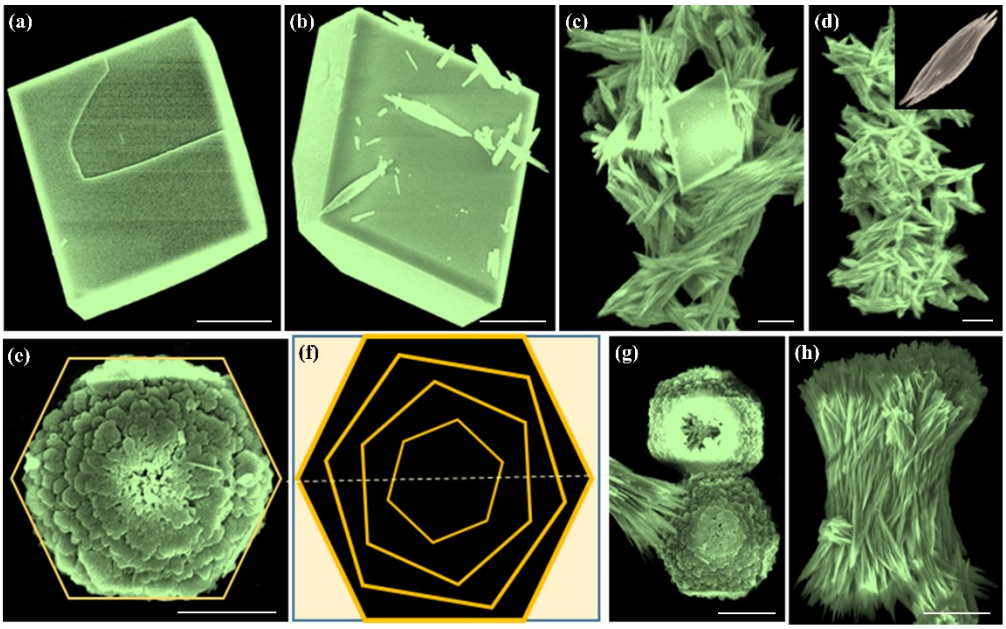

Fig. S5 (a-d) shows SEM images of mineralized particles induced by different concentrations of Mg^{2+} ((a), 0; (b), 0.01 mol·L^{-1}; (c), 0.02 mol·L^{-1}; (d), 0.03 mol·L^{-1}), (e), (g) and (h) are the SEM images of mineralized particles induced by different [Mg^{2+}] when CTAB concentration is 6 g·L^{-1} ((e), 0; (g), 0.01 mol·L^{-1}; (h), 0.03 mol·L^{-1}), (f) is the simulation diagram of the rotational layers of vaterite assembly. The scale bar stands for 5 μm.

Text S3: Effects of different Mg^{2+} and CTAB concentrations on morphology

If inductive factors are absent, the most common form of $CaCO_3$ mineralization is rhombohedral calcite (Fig. S5a). If the amount of [Mg^{2+}] is gradually increased, acicular aragonite mineralized particles begin to appear when [Mg^{2+}]/[Ca^{2+}] is 1:1 (Fig. S5b), dominate at a ratio of 3:1 (Fig. S5c), and are the only form at a ratio of 4:1 (Fig. S5d). The enlarged insert in Fig. S5d shows that, when only Mg^{2+} is used, the acicular aragonite particles obtained are a relatively simple aggregate formed of several primary particles with a diameter of about 100 nm that has no chiral characteristics. Hexagonal layered vaterite (Fig. S5e) is obtained from mineralization induced by CTAB alone, and each layer rotates at a certain angle, forming a chiral structure (Fig. S5f). If a low

concentration of Mg^{2+} ($[Mg^{2+}]/[Ca^{2+}]$=1:1) is added, a small amount of aragonite particles appear, and a higher-level assembly aggregation structure is formed (Fig. S5g). When $[Mg^{2+}]/[Ca^{2+}]$ is 3:1, aragonite particle aggregates dominate, and the number of primary acicular aragonite particles constituting the aggregates increases significantly. As the diameter of the primary particle decreases and the length increases--that is, as the ratio of length to diameter increases--the primary particle assembly tends to distort (Fig. S5h). Therefore, the shape of the aragonite is mainly the result of Mg^{2+} regulation, but Mg^{2+} alone cannot form an assembly of multiple structures, nor do the results show chiral characteristics. For mineralized particles of both aragonite and vaterite, CTAB promotes chiral assembly.

Fig. S6

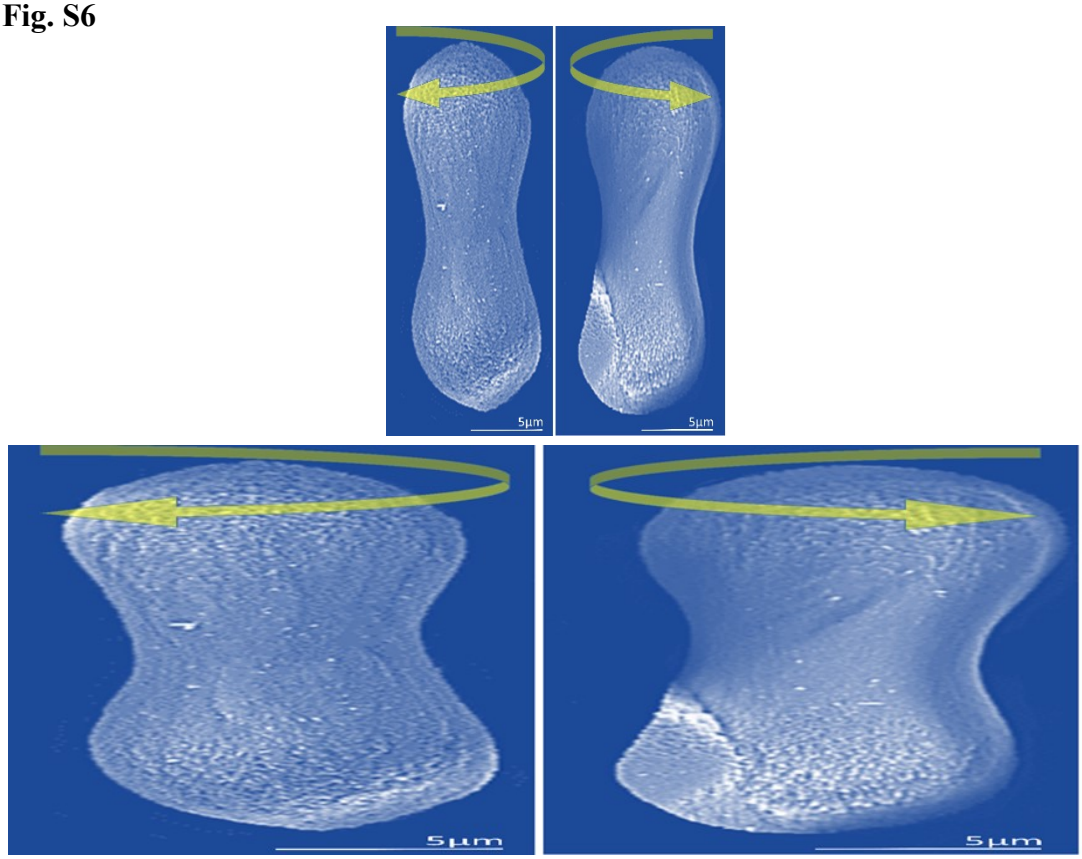

Fig. S6 SEM images of the two enantiomers of A-$CaCO_3$ (upper), and their horizontal triple magnification (down).

Fig. S7

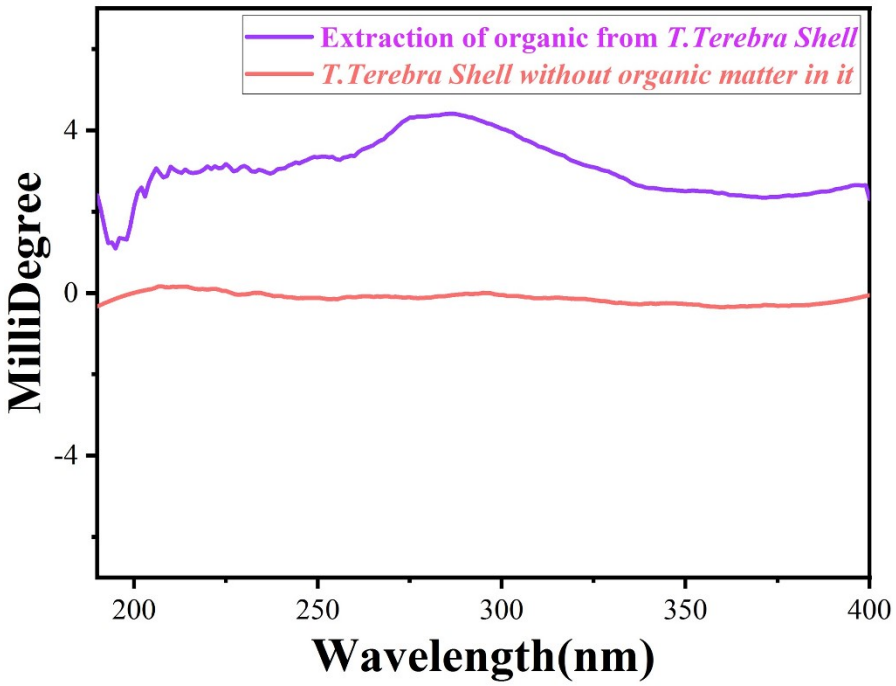

Fig. S7 CD Spectra of organic matter extracted from *Turritella terebra* Shell and *Turritella terebra* Shell without organic matter in it.

Fig. S8

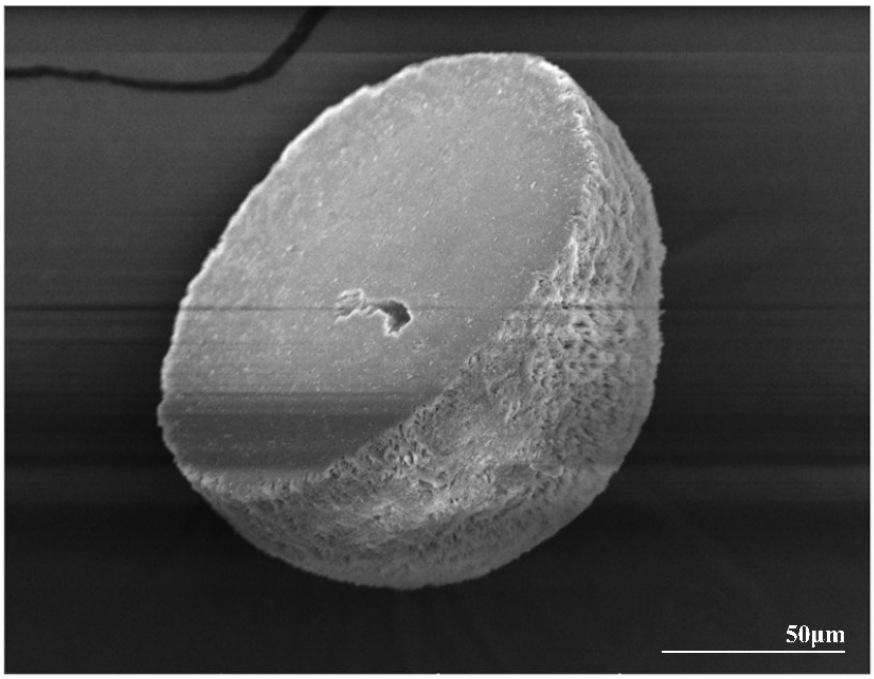

Fig. S8 An asymmetric spherical crown structure.

Fig. S9

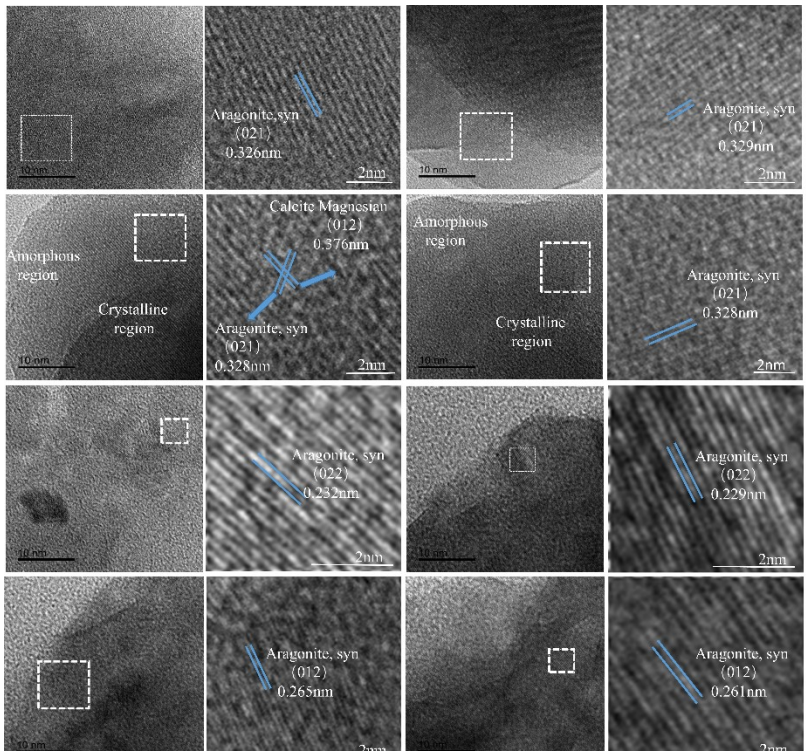

Fig. S9 HRTEM images of different crystal planes.

Fig. S10

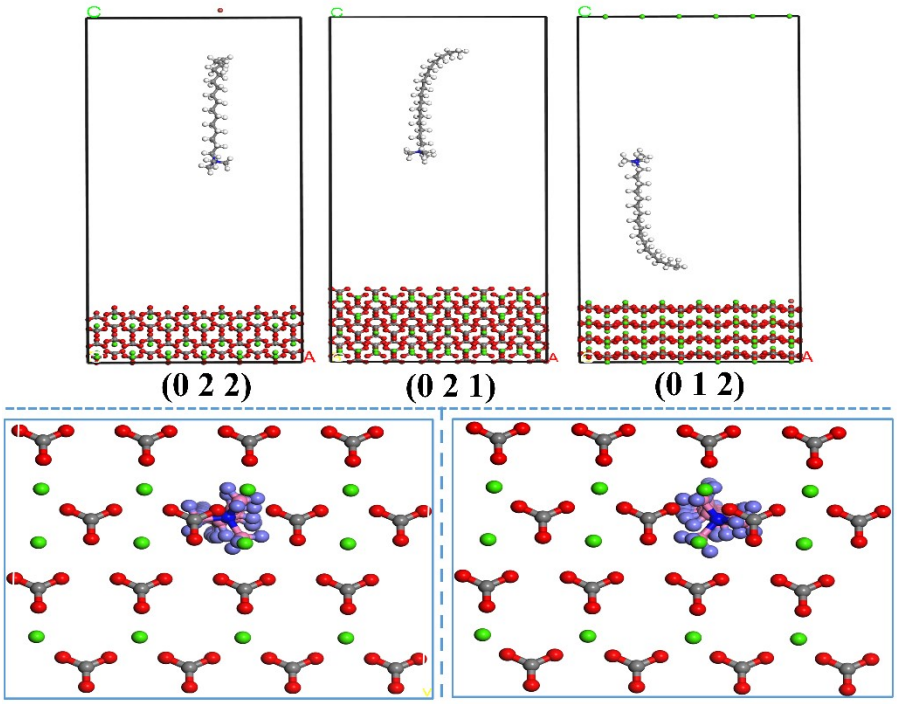

Fig. S10 Adsorption simulation of CTAB molecules on different aragonite crystal planes (upper) and chiral enantiomers formed by absorption of CTAB molecules on (0 2 2) crystal planes (upward view) (down).

Fig. S11

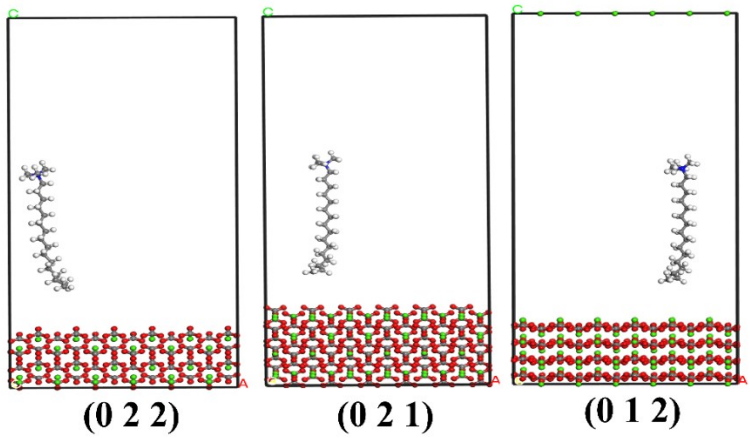

Fig. S11 Adsorption simulation of CTA^+ on different aragonite crystal planes.

Fig. S12

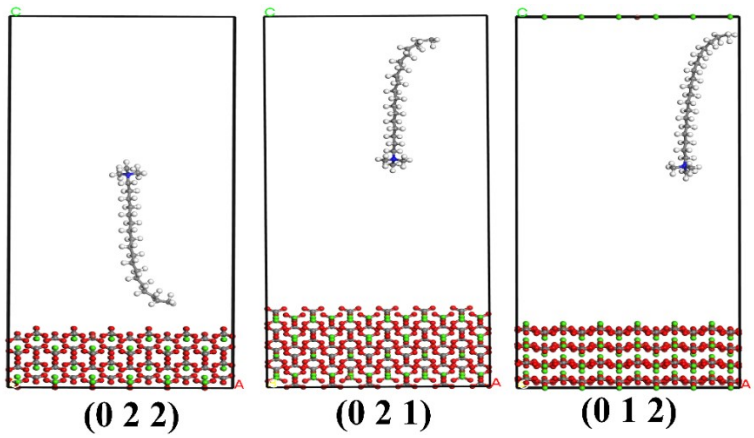

Fig. S12 Adsorption simulation of OTAB molecules on different aragonite crystal planes.

Fig. S13

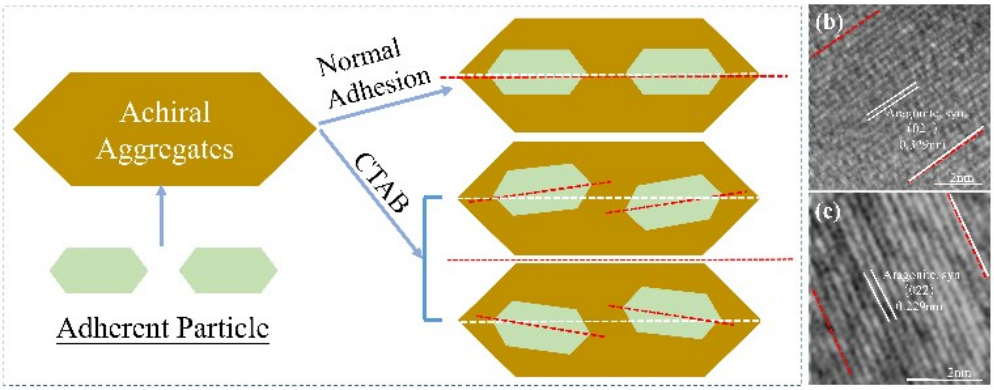

Fig. S13 (a) Schematic diagram of the deviation of "daughter" particles as they adhere to "mother" particles as caused by adsorption chirality (the size of the particles is not proportional to the real particles), and (b) and (c) HRTEM images of different crystal planes, In the (b) and (c) figures, the red solid line and the blue solid line are crystal planes at different positions, and the red dotted line is the translation line of the red solid line.

Table S1

Table S1 Binding energy and deformation energy of CTAB on different aragonite crystal planes.

Energy	**(0 2 2)**	**(0 2 1)**	**(0 1 2)**
Binding energy	-31167.8	-41900.3	-32406.8
Deformation energy	425.471	596.773	512.566

Note: All values are in $kJ \cdot mol^{-1}$

Table S2

Table S2 Energy of CTAB adsorbed on aragonite (0 2 2) crystal plane.

Crystal planes	Absorption energy(kJ·mol^{-1})	Rigid Absorption energy(kJ·mol^{-1})	Deformation energy(kJ·mol^{-1})
$CaCO_3$ (0 2 2)-1	-3.116732e+004	-3.159279e+004	425.47225031
$CaCO_3$ (0 2 2)-2	-3.116603e+004	-3.159967e+004	433.63437827
$CaCO_3$ (0 2 2)-3	-3.116453e+004	-3.160515e+004	440.61440485
$CaCO_3$ (0 2 2)-4	-3.116336e+004	-3.160549e+004	442.13616111
$CaCO_3$ (0 2 2)-5	-3.116180e+004	-3.160829e+004	446.48786429
$CaCO_3$ (0 2 2)-6	-3.115785e+004	-3.156097e+004	403.12626061
$CaCO_3$ (0 2 2)-7	-3.115644e+004	-3.157723e+004	420.78249979
$CaCO_3$ (0 2 2)-8	-3.115576e+004	-3.155667e+004	400.91003006
$CaCO_3$ (0 2 2)-9	-3.115509e+004	-3.157389e+004	418.79729002
$CaCO_3$ (0 2 2)-10	-3.114824e+004	-3.153988e+004	391.63804445

Table S3

Table S3 Energy of CTAB adsorbed on aragonite (0 2 1) crystal plane.

Crystal planes	**Absorption energy(kJ·mol^{-1})**	**Rigid Absorption energy(kJ·mol^{-1})**	**Deformation energy(kJ·mol^{-1})**
$CaCO_3$ (0 2 1)-1	-4.185818e+004	-4.250862e+004	596.76907409
$CaCO_3$ (0 2 1)-2	-4.191059e+004	-4.252256e+004	611.94541831
$CaCO_3$ (0 2 1)-3	-4.189443e+004	-4.248312e+004	588.67414214
$CaCO_3$ (0 2 1)-4	-4.189150e+004	-4.245445e+004	562.97027170
$CaCO_3$ (0 2 1)-5	-4.189041e+004	-4.250426e+004	613.84607492
$CaCO_3$ (0 2 1)-6	-4.186191e+004	-4.248045e+004	618.51062403
$CaCO_3$ (0 2 1)-7	-4.184411e+004	-4.243110e+004	586.97716992
$CaCO_3$ (0 2 1)-8	-4.160643e+004	-4.245290e+004	846.45986474
$CaCO_3$ (0 2 1)-9	-4.116460e+004	-4.301548e+004	1850.85602655
$CaCO_3$ (0 2 1)-10	-4.101436e+004	-4.203227e+004	1017.91791660

Table S4

Table S4 Energy of CTAB adsorbed on aragonite (0 1 2) crystal plane.

Crystal planes	Absorption energy(kJ·mol^{-1})	Rigid Absorption energy(kJ·mol^{-1})	Deformation energy(kJ·mol^{-1})
$CaCO_3$ (0 1 2)-1	-3.240989e+004	-3.292245e+004	512.56389019
$CaCO_3$ (0 1 2)-2	-3.240520e+004	-3.290051e+004	495.30952171
$CaCO_3$ (0 1 2)-3	-3.240430e+004	-3.289832e+004	494.01384551
$CaCO_3$ (0 1 2)-4	-3.240246e+004	-3.290272e+004	500.25811709
$CaCO_3$ (0 1 2)-5	-3.240088e+004	-3.289978e+004	498.90333634
$CaCO_3$ (0 1 2)-6	-3.239998e+004	-3.290156e+004	501.57826547
$CaCO_3$ (0 1 2)-7	-3.239729e+004	-3.289373e+004	496.44650375
$CaCO_3$ (0 1 2)-8	-3.239590e+004	-3.287724e+004	481.34554034
$CaCO_3$ (0 1 2)-9	-3.239525e+004	-3.287447e+004	479.22087025
$CaCO_3$ (0 1 2)-10	-3.239340e+004	-3.287721e+004	483.81034344

Table S5

Table S5 Bond length of different N-CH_3 bonds on the head group of CTA^+.

Bond	N1-C17(Å)	N1-C18(Å)	N1-C19(Å)
Pure CTAB	1.50768	1.49963	1.49963
(0 2 1)	1.50451	1.49904	1.49932
Difference	-0.00317	-0.00059	-0.00031
(0 2 2)	1.50539	1.49943	1.49940
Difference	-0.00229	-0.0002	-0.00023
(0 1 2)	1.50514	1.49963	1.49974
Difference	-0.00254	0	0.00011

Table S6

Table S6 Bond length of different N-CH_3 bonds on the head group of OTAB molecule.

Bond	N1-C19(Å)	N1-C20(Å)	N1-C21(Å)
Pure OTAB	1.50836	1.50032	1.49265
(0 2 1)	1.50050	1.49936	1.50533
Difference	-0.00786	-0.00096	0.01268
(0 2 2)	1.49986	1.49973	1.50691
Difference	-0.0085	-0.00059	0.01426
(0 1 2)	1.50111	1.50031	1.50811
Difference	-0.00725	-0.00001	0.01546

Reference

1 M. B. Gindele, L. V. Steingrube, D. Gebauer, *CrystEngComm,* 2021, **23**, 7938-7943.

2 J. W. Morse, R. S. Arvidson, A. Luttge, *Chem. Rev.,* 2007, **107**, 342-381.

3 M. Aoki, T. Matsuda, Y. Tomo, Y. Miyata, M. Inoue, T. Kigawa, S. Yokoyama, *Protein Expression Purif.,* 2009, **68**, 128-136.

4 B. B. Mandal, S. C. Kundu, *Biotechnol Bioeng,* 2008, **99**, 1482-1489.

5 C. La Mesa, *J. Colloid Interface Sci.,* 2005, **286**, 148-157.

6 R. L. C. Akkermans, N. A. Spenley, S. H. Robertson, *Mol. Simul.,* 2013, **39**, 1153-1164.

7 T. Semoto, Y. Tsuji, K. Yoshizawa, *Bull. Chem. Soc. Jpn.,* 2012, **85**, 672-678.